Eur. Phys. J. B **11**, 445–453 (1999)

THE EUROPEAN PHYSICAL JOURNAL B

EDP Sciences

Surface reorientation dynamics of nematic liquid crystals

S. Faetti[1], M. Nobili[2,a], and I. Raggi[1]

[1] INFM and Dipartimento di Fisica, Universita di Pisa, Via Buonarroti ed.B 2, 56126 Pisa, Italy
[2] Groupe de Dynamique des Phases Condensées[b], Université de Montpellier II, Place E. Bataillon, 34000 Montpellier, France

Received 7 December 1998

Abstract. In this paper we report an experimental investigation on the dynamics of the azimuthal director reorientation at a nematic-solid interface. Three qualitatively different kinds of substrates have been investigated: I) intrinsically anisotropic SiO-substrates (60°-evaporation), II) isotropic SiO-substrates (0°-evaporation) and III) rubbed PVA-substrates. In the case II), an in-plane anisotropy was induced cooling slowly the thermotropic nematic liquid crystal (NLC) from the isotropic phase in the presence of a 0.75 T magnetic field. The reorientation dynamic of the surface azimuthal director angle at the switching-on and off of a magnetic (or electric) field has been investigated. All the substrates show comparable azimuthal anchoring energies and two dynamic regimes: a fast dynamic response, driven by the bulk director reorientation and an extremely slow reorientation. The slow dynamics is explained in terms of anisotropic adsorption of NLC molecules on the solid substrate and is well represented by a stretched exponential.

PACS. 61.30.Gd Orientationnal order of liquid crystals; electric and magnetic field effects on order – 78.20.Ci Optical constants: refractive index, complex dielectric constant, absorption, reflexion and transmission coefficients, emissivity

1 Introduction

The macroscopic properties of nematic liquid crystals are described by the director $\mathbf{n}$ which represents the average orientation of the liquid crystal molecules [1]. In absence of external torques, the surface director $\mathbf{n}_s$ is oriented along the easy axis $\mathbf{n}_0$ that corresponds to a minimum of the anchoring energy $W(\mathbf{n}_s, \mathbf{n}_0)$ [2,3]. The surface director orientation is defined by two angles: the surface polar angle θ_s with respect to the normal to the interface and the surface azimuthal angle φ_s with respect to an axis on the surface plane. If the surface azimuthal angle is fixed, $W(\mathbf{n}_s, \mathbf{n}_0)$ is a function of the surface polar angle only and is called polar anchoring energy. On the other hand, by keeping fixed the polar angle, $W(\mathbf{n}_s, \mathbf{n}_0)$ is a function of the surface azimuthal angle only and is called azimuthal anchoring energy [3].

Here we focalize our attention on the azimuthal anchoring of thermotropic nematic liquid crystals (NLC). Two basic mechanisms have been proposed to explain the azimuthal anchoring. The first one is due to the direct van der Waals interactions between the NLC and the anisotropic molecules of the substrate. Such a mechanism is probably responsible for the azimuthal anchoring on rubbed polymeric layers where the long polymeric chains are aligned along the rubbing direction [4]. The second mechanism has been proposed by Berreman [5] to explain the anchoring on grooved substrates (obliquely evaporated SiO and holographic gratings). He showed that, if the interactions with the substrate favor a planar director alignment with a strong polar anchoring, the elastic free energy is minimized when the surface director is aligned along the grooves. Such an elastic model has also been generalized to account for the effects of a weak polar anchoring [6]. However, these two anchoring mechanisms cannot explain all the experimental observations. In particular, it is known that a stable azimuthal anchoring can be induced in an isotropic substrate if the NLC is introduced in a cell flowing parallel to the substrate or if the NLC is slowly cooled from its isotropic phase in the presence of an orienting magnetic (or electric) field [7–9]. Both these phenomena can be explained assuming that the NLC molecules which are oriented by the flow or by the external field are anisotropically adsorbed on the substrate. It results an azimuthal anchoring due to the interactions between the adsorbed molecules and the bulk nematic molecules. A contribution of the absorption to the anchoring energy is expected to be present also in the case of the standard anisotropic substrates (polymeric rubbed substrates, SiO-treated substrates, holographic gratings...).

The relevance of the absorption for the azimuthal anchoring is also reflected by the very peculiar dynamics of the azimuthal director angle [10–15]. In the literature, the surface dynamics of the director is usually described introducing a surface viscosity coefficient γ_s in analogy with the γ-bulk orientational viscosity [16].

[a] e-mail: nobili@gdcp.univ-montp2.fr
[b] UMR CNRS/UMII 5581

From a simple dimensional analysis, one expects $\gamma_s = \gamma L_{int}$, where L_{int} is a characteristic microscopic interfacial length which can depend on the surface director orientation. A model for the surface viscosity has been recently reported in reference [17]. However, the surface viscosity is not sufficient to explain the complex dynamics of the director azimuthal angle, and, in particular, the ultra-slow relaxation of the azimuthal director angle which has been observed both with lyotropic and thermotropic nematic liquid crystals [10–15,18]. The slow dynamics in lyotropic liquid crystals can be explained in terms of peculiar features of this kind of media as well as defects in the micellar structure [11] or dry friction at the surfaces [18]. Both these mechanisms are absent in thermotropic nematic liquid crystals. In particular, no static friction has been observed in the experiments with NLCs [19]. The slow dynamics in NLCs has been usually ascribed to adsorption of nematic molecules at the interfaces. Then, the study of the surface dynamics should give important insights on the adsorption and on its influence on the azimuthal anchoring.

In this paper we present a direct dynamic measurement of the azimuthal reorientation of the director on SiO-substrates and PVA-substrates rubbed along a given direction. Both 60° and 0°-evaporation angles were used for the SiO deposition. The 60°-evaporated SiO substrates and the rubbed PVA substrates give a planar homogeneous alignment along an axis in the surface plane, while, the 0°-evaporated SiO substrates result in a planar degenerate anchoring [20]. In order to induce an in-plane anisotropy on these latter substrates, we applied a 0.75 T magnetic field parallel to the substrates and we cooled slowly the NLC from the isotropic phase. This procedure leads to a planar easy axis along the magnetic field. The large part of the measurements have been performed using the sensitive reflectometric method which has been described in a recent paper [21]. This method provides a direct and automated measurement of the surface director azimuthal angle within $0.1 - 0.2°$ with a sensitivity better than 0.01°. In some cases we have also used a transmission light method and a different reflectometric method to measure simultaneously the fast dynamics of the surface elastic torque and of the surface director. An external magnetic field (or electric field) is applied parallel to the substrate in order to exert a desorienting azimuthal torque on the director. Then, a twist director distortion occurs in the bulk which induces a surface elastic torque and a consequent azimuthal rotation of the director in the plane of the surface. For all the investigated substrates, comparable anchoring energies and similar dynamic behaviors are measured. Two dynamic regimes are observed: a fast reorientation, with the surface director $\mathbf{n}_s$ which follows the relaxation of the surface elastic torque, and an ultra-slow continuous reorientation which occurs when the surface elastic torque has reached its equilibrium value. Preliminary observations on these two dynamic regimes were already reported in [15] for the interface between a NLC and a 60°-obliquely evaporated SiO-layer. Slow dynamic relaxations at the surface of NLCs have also been reported in references [10–14].

The plan of the paper is the following: in Section 2 we describe the experimental procedures and the set up used to investigate the fast dynamic regime. In Section 3 we study the fast reorientation dynamics. We show that this dynamic regime is in a good quantitative agreement with the predictions of the classical theory of the director anchoring for a negligible surface viscosity. In Section 4 we describe briefly the reflectometric method used to study the ultra-slow dynamics and we show the related experimental results. This regime, which cannot be explained in terms of the standard dynamic models, is ascribed to anisotropic absorption of nematic molecules on the substrate. The observation of the same kind of dynamic behavior on all the investigated substrates suggests that the absorption of nematic molecules on a substrate represents a very general mechanism for the azimuthal anchoring. Finally, Sections 5 and 6 are devoted to discussion and conclusions, respectively.

2 Experimental procedures

The nematic liquid crystal is 4-pentyl-4'-cyanobyphenil (5CB) which has a positive dielectric anisotropy $\Delta\epsilon$ and shows a nematic-isotropic transition at the temperature $T_c = 35.3°$. The nematic sample is enclosed in a wedged cell made with two glass plates separated by two mylar spacers of different thicknesses. The average cell thickness is 180 μm and the wedge angle is about 0.5°. The glass plates, too, have a wedge-shape with a wedge angle $\approx 0.5°$. Wedges are needed to separate the optical beams reflected by the different interfaces of the cell. Both plates give a planar homogeneous anchoring ($\theta_s = \pi/2$, $\varphi_s = 0$) along the x-wedge axis. Due to the smallness of the nematic wedge angle, the local thickness of the nematic is virtually constant on the lighted region (0.5 mm-diameter). Then, the system is virtually equivalent to a nematic slab confined between two parallel surfaces in $z = 0$ and $z = d \approx 180$ μm with a planar easy axis along $\hat{\mathbf{x}}$.

Two different treatments of the glass plates are used: evaporation of SiO and coating by a thin layer of polivynil alcohol (PVA) followed by rubbing [20]. Two SiO-evaporation angles are used: 60° and 0°, respectively. It is known [22] that in the first case (60°), the director is aligned along a given axis in the plane of the substrate (*homogeneous planar alignment*), while in the second case (0°) the director still lies in the surface plane but there is no easy direction on it (*degenerate planar alignment*). A planar homogeneous alignment is induced on the 0°-evaporated SiO substrates using the following procedure: the NLC is introduced in the cell in the isotropic phase ($T = 40$ °C) and in the presence of a 0.75 T magnetic field parallel to the wedge axis. Then, the NLC is slowly cooled in the nematic phase (typically $\mathrm{d}T/\mathrm{d}t < 1°$/hour). Finally, the magnetic field is switched off. As a result, a homogeneous orientation along the direction of the magnetic field is obtained. An oven with a temperature-stability and control of 0.01 °C is used.

Two parallel aluminium stripes are inserted between the two glass plates of the cell at a distance of 4 mm to

apply an AC electric field **E** (frequency $\nu = 1$ kHz) in the plane of the substrates and nearly orthogonal to the easy axis. Due to the positive dielectric anisotropy, the director tends to be aligned along the direction of the electric field, and a director twist occurs close to the interfaces of the NLC. The consequent surface elastic torque induces a rotation of the director at the surface.

The experiment consists on measuring the surface director azimuthal angle versus time after the switching on and off of the electric field. The fast director dynamics is studied using the reflectometric method described in reference [23]. A polarized He - Ne laser beam impinges at almost normal incidence on the cell. We measure the intensities of three reflected beams that we denote by (1), (2) and (3), respectively. Beam (1) is reflected from the first glass-nematic interface, passes through a crossed analyzer and finally, is detected by a photodiode. The output signal of the photodiode is amplified and sent to one input channel of a digital signal analyzer (Data Precision 6100). If the characteristic length of the director distortion is much greater than the optical wavelength, intensity $I_{(1)}$ is given by [23]:

$$I_{(1)} = I_0 \sin^2[2(\delta - \varphi_{\rm s})], \tag{1}$$

where δ is the angle between the polarization plane of the incident beam and the **x**-easy axis, and $\varphi_{\rm s}$ is the angle of the surface director with the easy axis. I_0 is proportional to the intensity of the incident beam. According to equation (1), a rotation $\varphi_{\rm s}$ of the surface director from the easy axis induces a variation of the reflected intensity. To have the maximum sensitivity to small surface director rotations we set $\delta = \pi/8$ and we measure the corresponding intensity $I_{(1)}(\pi/8) = I_0/2$ ($\varphi_{\rm s} = 0$ in absence of the electric field). Then, we switch on the electric field and we measure the reflected intensity versus time. The ratio between the measured intensity and $I_{(1)}(\pi/8)$ provides a direct measurement of the instantaneous surface director azimuthal angle $\varphi_{\rm s}$. For $\varphi_{\rm s} \ll \pi/8$, the variation of the reflected intensity is virtually proportional to $\varphi_{\rm s}$.

An independent and complementary information on the surface dynamics is obtained looking at the beam which is transmitted across the wedge-cell and is reflected back in the cell by the second glass-air interface. In absence of a director twist, this beam gives origin to two different reflected beams: the extraordinary and the ordinary beam. A third reflected beam appears if a twist distortion of characteristic length ξ is present in the cell [24]. This beam, which we call (2), is due to the failure of the adiabatic approximation and its properties have been explained satisfactorily using the theoretical approach developed in reference [25]. Beam (2) sees an average index $n_{\rm av} = (n_{\rm o} + n_{\rm e})/2$ and is spatially separated from the extraordinary and ordinary beams due to the wedge of the cell ($n_{\rm o}$ and $n_{\rm e}$ are the ordinary and the extraordinary indices of the nematic LC). Simple analytical expressions for the intensity of the non-adiabatic beam were obtained in reference [24] for $\lambda/\xi \ll 1$, where λ is the optical wavelength. A good agreement between theory and experiment was obtained. For $\lambda/\xi \ll 1$, the intensity $I_{(2)}$ of beam (2) is given by

$$I_{(2)} = A \left(\left.\frac{\partial \varphi}{\partial z}\right|_{z=0} - \left.\frac{\partial \varphi}{\partial z}\right|_{z=d} \right)^2, \tag{2}$$

where A is a constant which depends on the optical parameters of the nematic liquid crystal and of the substrate. For a nematic cell having the same easy axes and anchoring energies on the two interfaces, $\varphi(z)$ is an even function with respect to the center of the cell ($z = d/2$) and the two z-derivatives appearing in equation (2) are equal and opposite. In this special case, $\sqrt{I_{(2)}}$ is simply proportional to $\left.\frac{\partial \varphi}{\partial z}\right|_{z=0}$. This means that $\sqrt{I_{(2)}}$ is proportional to the surface elastic torque acting on the director at the surface $z = 0$:

$$\Gamma_{\rm s} = K_{22} \left.\frac{\partial \varphi}{\partial z}\right|_{z=0} \tag{3}$$

where K_{22} is the twist elastic constant of the nematic LC. In order to be insensitive to fluctuations of the intensity of the laser beam, we measure also the intensity $I_{(3)}$ of a third beam (beam(3)) reflected by the first air-glass interface. $I_{(3)}$ is proportional to the intensity of the incident laser beam. Then, the ratios $I_{\rm I} = I_{(1)}/I_{(3)}$ and $I_{\rm II} = I_{(2)}/I_{(3)}$ are measured using the Signal Analyzer Data 6100. This procedure makes possible to obtain the surface angle $\varphi_{\rm s}$ and a signal proportional to the surface elastic torque $\Gamma_{\rm s}$ at the same time t.

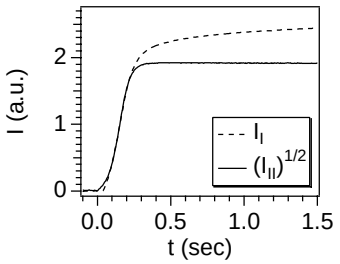

Fig. 1. $I_{\rm I}$ and $\sqrt{I_{\rm II}}$ *versus* time for a 60°-evaporated SiO substrate. The electric field is switched on at $t = 0$. The unities on the vertical axis are arbitrary. $\sqrt{I_{\rm II}}$ is proportional to the surface elastic torque and $I_{\rm I}$ is proportional to $\varphi_{\rm s}$.

3 The fast dynamic regime

A typical dynamic behavior of $I_{\rm I}$ and $\sqrt{(I_{\rm II})}$ at the switching on of the external electric field is shown in Figure 1. The electric field ($E = 300$ V/cm rms) is almost orthogonal to the easy axis and is switched on at time $t = 0$. The nematic cell is made with two SiO-treated glass plates at a 60°-evaporation angle and is kept at the temperature $T = 23$ °C. Different arbitrary unities have been used for the vertical scale of the two curves. As shown in Figure 1, with a proper choice of these unities, is possible to obtain a satisfactory superposition of the two curves during the first transient ($t < 0.2$ s). Since $\sqrt{I_{\rm II}}$ is virtually proportional to the surface elastic torque $\Gamma_{\rm s}(t)$ and $\Delta I_{\rm I}(t) \propto \varphi_{\rm s}(t)$, we infer that $\varphi_{\rm s}(t)$ follows practically without any delay the surface elastic torque during the first

transient. The small residual differences between the two signals in this first transient can be ascribed to a not perfect parallelism between the easy axes on the two surfaces of the nematic cell. Indeed, according to equation (2), $\sqrt{I_{\rm II}}$ is really proportional to the average of the torques (in modulus) at the two interfaces of the NLC, while $I_{\rm I}$ is related to the director orientation at the first glass-nematic interface only. Then, a small difference between the time-dependencies of the two intensities is expected if there is no perfect parallelism between the easy axes on the two surfaces of the nematic cell. Moreover, the sign of the difference is expected to change if the light beam impinges first on the second glass - nematic interface. This is just the behavior which is experimentally observed.

For $t > 0.2$ s, the two curves in Figure 1 have a completely different shape. In particular, the surface elastic torque ($\sqrt{I_{\rm II}}$) reaches an equilibrium value, while the surface azimuthal angle ($I_{\rm I}$) exhibits a very slow continuous increase. This means that $\varphi_{\rm s}(t)$ continues to orient toward the field direction while the applied elastic surface torque $\Gamma_{\rm s}(t)$ remains virtually constant. The same kind of behavior has been observed for all the other substrates (0°-SiO layer and rubbed PVA) independently of the temperature. Analogous fast and slow dynamic regimes are observed at the switching off of the electric field. The rising time of the fast dynamic regime at the switching on of the electric field is proportional to $1/E^2$.

The fast reorientation dynamics is in a good agreement with the predictions of the classical theory of the director anchoring and of the surface dynamic friction. When an electric field $\mathbf{E}$ much greater than the Freederickz threshold is switched on, a twist distortion is generated. The dynamic equation for the bulk director angle $\varphi(z)$ with respect to the $\hat{\mathbf{x}}$-axis is given by [1]:

$$\xi_{\rm E}^2 \frac{\partial^2 \varphi}{\partial z^2} + \sin\varphi\cos\varphi = \tau_{\rm b}\frac{\partial \varphi}{\partial t}, \tag{4}$$

where $\xi_{\rm E} = \sqrt{4\pi K_{22}/\Delta\epsilon}(1/E)$ is the electric coherence length [1], and $\tau_{\rm b}$ is a characteristic bulk relaxation time given by

$$\tau_{\rm b} = \frac{\gamma_1}{K_{22}}\xi_{\rm E}^2. \tag{5}$$

γ_1 is the bulk rotational viscosity. For $\varphi_{\rm s}(t) \ll 1$, the surface director angle satisfies the equation:

$$\frac{L}{K_{22}}\Gamma_{\rm s}(t) - \varphi_{\rm s}(t) = \tau_{\rm s}\frac{\partial \varphi_{\rm s}}{\partial t}, \tag{6}$$

where $\Gamma_{\rm s}(t)$ is the surface elastic torque defined in equation (3) and we have used the parabolic approximation for the azimuthal anchoring energy $W = K_{22}/(2L)\,\varphi_{\rm s}^2$ (L is the anchoring extrapolation length [16]). $\tau_{\rm s}$ in equation (6) is a characteristic surface relaxation time given by:

$$\tau_{\rm s} = \frac{\gamma_{\rm s}}{K_{22}}L, \tag{7}$$

where $\gamma_{\rm s} \approx \gamma_1 L_{\rm int}$ is the surface viscosity, and $L_{\rm int}$ is a characteristic interfacial length. $L_{\rm int}$ is expected to be of the order of the nematic coherence length which is typically $\xi \approx 2$ nm far from the nematic-isotropic transition temperature and $\xi \approx 10$ nm at the transition temperature [26]. Equation (6) shows that the response of the surface angle $\varphi_{\rm s}(t)$ is delayed by a time $\tau_{\rm s}$ with respect to the surface torque $\Gamma_{\rm s}(t)$. The surface dynamics depends greatly on the ratio between $\tau_{\rm b}$ and $\tau_{\rm s}$. Using the known values $\gamma_1 \approx 1$ p [27], $K_{22} \approx 3 \times 10^{-7}$dyne [28], $L_{\rm int} \approx \xi \approx 2$ nm [29], $\Delta\epsilon \approx 12$ [30] of the material constants of 5CB at room temperature and the extrapolation length $L \approx 100$ nm [15] for the SiO-nematic interface at room temperature, we find $\gamma_{\rm s} \approx 2 \times 10^{-7}$ p cm and $\tau_{\rm s} \approx 10^{-5}$ s. Using the experimental value $E = 300$ V/cm, we find $\xi_{\rm E} \approx 1.6$ μm and $\tau_{\rm b} \approx 0.1$ s, which is many order of magnitude larger than $\tau_{\rm s}$. In this condition, the rigth-hand side in equation (6) can be disregarded and $\varphi_{\rm s}(t)$ is given by the adiabatic approximation:

$$\varphi_{\rm s}(t) = \frac{L}{K_{22}}\Gamma_{\rm s}(t). \tag{8}$$

Then, $\varphi_{\rm s}(t)$ follows the surface elastic torque which is characterized by the bulk characteristic time $\tau_{\rm b}$ proportional to $1/E^2$, in agreement with the experimental observations.To make a quantitative analysis, we have solved numerically equations (4) and (8) and compared the theoretical predictions with the experiment in the first dynamic regime. Using the values of the material parameters of 5CB reported in the literature [15,27,28,30], we obtained a satisfactory quantitative agreement between the experimental and the numerical curves for any value of the electric field ($0 < E < 500$ V/m). Then, the fast dynamic behavior is well explained by equations (4), (8). On the opposite, it is evident that the slow dynamic regime is in a complete disagreement with the predictions of equation (8). Then, a different model is needed to explain the slow dynamic regime.

4 The slow dynamic regime

4.1 Experimental procedures

In this section we report the results concerning the slow reorientation regime. In this regime the surface director angle changes very slowly and continuously without reaching apparently a stationary value (a slow continuous drift is still observed after a few days). Variations of the surface azimuthal angle smaller than 0.1°/hour are currently measured. Then, any source of spurious drifts of the experimental signals has to be avoided. A possible drift-source is given by the Joule heating due to the electric field. For this reason the measurements of the slow dynamics have been made using a magnetic field in place of the electric field. Furthermore, a slightly different reflectometric method based on a lock-in technique has been used. This method is more accurate than the previous one and leads to a great reduction of spurious drifts. Details of the experimental method can be found in reference [21], here we only recall the main features.

The incident laser beam is polarized by a polarizer which rotates at the angular frequency $\omega = 0.5236$ rad/s

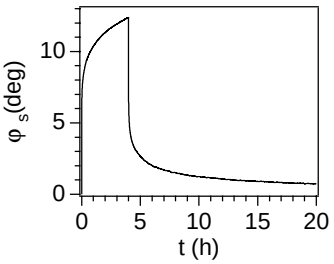

Fig. 2. Dynamic behavior of the surface director angle φ_s for a 60°-evaporated SiO substrate. The thickness of the SiO-layer is 4nm. A magnetic field $H = 0.75$ T is switched on at time $t = 0$ and switched off at $t = 4$ h.

and the intensity $I(t)$ of the beam reflected by the first solid-nematic interface is measured by a photodiode. $I(t)$ is given by [21]:

$$I(t) = I_o[a + b\cos 2(\omega t - \varphi_s)] \tag{9}$$

where I_o is the intensity of the incident beam, a and b are constant coefficients which depend on the geometry of the interface and on the optical material parameters of the NLC and of the substrate, and ωt is the instantaneous angle between the polarizer axis and the $\mathbf{x}-$*easy axis*. A reference signal is obtained from the beam which is reflected at the first air-glass isotropic interface of the nematic wedge-cell. This beam passes through an analyzer and is collected by a photodiode. The output of the photodiode oscillates at the angular frequency 2ω with a phase which can be changed by a rotation of the analyzer. A home computer performs the Fourier transform of both signals at the frequency 2ω and calculates the phase difference $\Delta\phi$. Before the switching on of the magnetic field, the analyzer is rotated in such a way to get $\Delta\phi = 0$. Then, the magnetic field is switched on and $\Delta\phi(t)$ is measured. The corresponding surface azimuthal angle is $\varphi_s(t) = \Delta\phi(t)/2$. This method provides an absolute accuracy on the measurement of φ_s better than 0.2° on the whole angular range $0 - 360°$ and better than 0.03° for surface director rotations smaller than 5°. With the room thermostated within 0.2 °C, the residual drift of the experimental signal is lower than 0.02°/hour.

4.2 Experimental results

Figure 2 shows a typical behavior of the surface director angle at the temperature $T = 31$ °C for a thin SiO-layer (thickness ≈ 4 nm) evaporated at a 60°-incidence. A magnetic field $H = 0.75$ T is switched on at time $t = 0$ and switched off at $t = 4$ h. At the switching on, the director angle reaches rapidly the "*anchoring amplitude*" $\varphi_a \approx 6.5°$ which corresponds to the surface director rotation straight after the fast dynamic regime. According to the theoretical analysis in Section 3, φ_a satisfies equation (8) with $\Gamma_s(t)$ which has to be replaced by the equilibrium elastic torque $\Gamma_s \approx K_{22}/\xi_H$, where $\xi_H = (K_{22}/\chi_a H^2)^{1/2}$ and χ_a is the anisotropy of the magnetic susceptibility [1]. Then, the anchoring amplitude is proportional to the extrapolation length of the substrate ($\varphi_a \approx L/\xi_H$). After

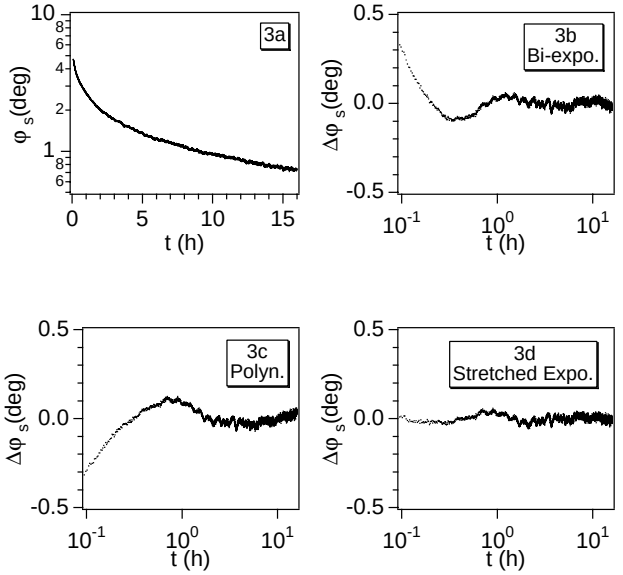

Fig. 3. (a) φ_s *versus* time after the switching off of the magnetic field. The experimental points are the same as in Figure 2 but $t = 0$ represents here the switching off time. Points at $t < t_{cut} = 342$ s have been discarded. (b-d) Difference $\Delta\phi_s$ between the experimental values of ϕ_s and the best fit values: (b) bi-exponential (Eq. (10)), (c) polynomial (Eq. (11)), (d) stretched exponential (Eq. (12)).

the fast transient, the director angle shows a very slow increase which persists also after a few days. An analogous behavior is observed at the switching off of the magnetic field: a fast relaxation of amplitude $-\varphi_a$ is followed by a slow reorientation toward the easy axis. Here we are interested to study the slow dynamic regime, then those experimental points which correspond to the fast transient have to be rejected from the analysis of the experimental data. According to Section 3, the fast dynamic regime is characterized by the bulk relaxation time τ_b. Then, the experimental points occurring at times lower than a cutting time $t_{cut} \approx 3\tau_b$ have to be discarded. At the switching on and well above the Freederickz threshold, the bulk relaxation time is $\tau_b = \gamma_1 \xi_H^2/K_{22} = \gamma_1/(\chi_a H^2)$. The dynamics after the switching off is more complex because the spatial harmonics of the initial director distortion decay with different characteristic times. The slowest bulk relaxation time corresponds to the decay of the fundamental spatial mode and is given by $\tau_b = \gamma_1 d^2/(K_{22}\pi^2) \approx 100$ s [31].

Figure 3a shows the director azimuthal angle φ_s versus time t after the switching off of the magnetic field. The experimental points are the same as in Figure 2 but $t = 0$ represents now the switching off time and points at times $t < t_{cut} = 342$ s $\approx 3\tau_b$ have been removed. The non-linearity of the semi-logarithmic plot in Figure 3a evidences a strongly non-exponential behavior. Three different time-laws have been compared with the experimental results. They consist of the bi-exponential

$$\varphi_s(t) = A + B\exp\left(\frac{t}{\tau_1}\right) + C\exp\left(\frac{t}{\tau_2}\right), \tag{10}$$

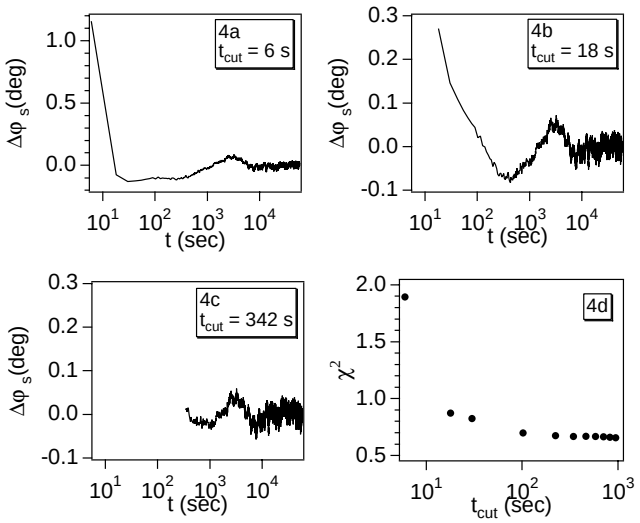

Fig. 4. (a-c) Residues $\Delta\varphi_s$ for the stretched exponential at the switching off of the magnetic field for different values of the cutting time t_{cut}. (a) $t_{cut} = 6$ s, (b) $t_{cut} = 18$ s, (c) $t_{cut} = 342$ s, (d) χ^2 *versus* the cutting time.

the polynomial

$$\varphi_s(t) = A + Bt^{\gamma}, \tag{11}$$

and the stretched exponential

$$\varphi_s(t) = A \exp\left[-\left(\frac{t}{\tau}\right)^{\alpha}\right] + B. \tag{12}$$

The polynomial and the stretched exponential are typical of complex systems which are characterized by a distribution of time scales as, for instance, glass forming materials. Figures 3b, 3c and 3d show the residuals $\Delta\varphi_s$ between the experimental data in Figure 3a and the best fit curves corresponding to the time-laws in equations (10), (11) and (12), respectively. The stretched exponential exhibits the best agreement with the experiment. Analogous results are obtained at different temperatures and magnetic fields.

Figures 4a, 4b and 4c show $\Delta\varphi_s$ in the case of a stretched exponential for some different values of t_{cut}. The corresponding χ^2 *versus* t_{cut} is shown in Figure 4d. As expected, χ^2 reaches a virtually constant minimum value when $t_{cut} > t' \approx 3\tau_b \approx 300$ s, with t' independent of the magnetic field intensity. The same behavior is observed at the switching on of the magnetic field. In this latter case, t' is proportional to $1/H^2$ and becomes negligible (with respect to the acquisition time $t = 12$ s) at the higher magnetic fields ($H > 0.1$ T). These results confirm that the slow and fast dynamic regimes are related to different mechanisms.

Unfortunately, the best fit parameters α and τ of the stretched exponential are obtained with a very large uncertainty. Indeed, appreciably different values of coefficients α and τ in equation (12) lead to nearly identical curves in the time interval [0.1 h,15 h]. The best fit with the stretched exponential law needs a simultaneous information on a large range of time scales: more decades

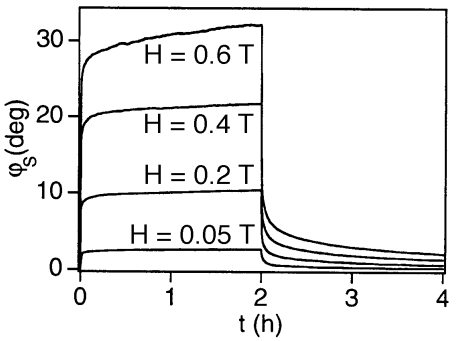

Fig. 5. Surface azimuthal angle φ_s *versus* time for different values of the amplitude of the applied magnetic field. The thickness of the a 60°-evaporated SiO layer is 4 nm and the temperature of the nematic sample is $T = 35$ °C . The magnetic field is switched on at $t = 0$ and switched off at $t = 2$ h.

of the signal $\varphi_s(t)$ and, thus, a very longer measurement time (months) is needed to obtain accurate best fit parameters. Furthermore, α and τ are very sensitive to the tails of the curves where small residual drifts of the signals play an important role. Then, a systematic investigation of the dependence of the best fit parameters on the temperature and on other external parameters resulted so far very inaccurate.

Figure 5 shows the time-response of the surface azimuthal angle φ_s at the temperature $T = 35$ °C for different values of H. The magnetic field is switched on at $t = 0$ and switched off at $t = 2$ h. The SiO-substrate is the same as in Figure 2. For $t > t_{cut}$, the ratio $\varphi_s(t, H)/\varphi_s(t, H = 0.05\text{ T})$ is proportional to the magnetic field and is independent of time. Then, $\varphi_s(t, H) \approx aHf(t)$, where a is a constant coefficient and $f(t)$ is a function of time. This means that the characteristic relaxation times of the slow dynamic regime are virtually independent of the magnetic field intensity, at least for small enough surface director desorientations.

A slow dynamic regime with analogous features is also present for the PVA rubbed substrates and for the 0°-evaporated SiO substrates. In the latter case, a planar homogeneous alignment along a given **x**-axis in the substrates plane was induced by cooling slowly (0.5 h) the NLC from the isotropic phase toward the nematic one in the presence of a 0.75 T magnetic field. Observation of the 5CB-cell with a polarizing microscope showed a good homogeneous alignment. The induced alignment is stable against nematic-isotropic-nematic thermal cycles. Long times (≈ 50 h) of permanence of the sample in the isotropic phase are needed to observe the occurrence of strong surface inhomogeneities meaning that the memory of the induced surface anisotropy is a strong effect.

Figure 6 shows a comparison between the slow dynamic regimes for the different substrates (Fig. 6a: 60°-SiO, Fig. 6b: 0°-SiO, Fig. 6c: rubbed PVA) at the same temperature ($T = 30$ °C) and magnetic field amplitude ($H = 0.75$ T). The 0°-SiO layer and the 60°-SiO layer are ≈ 15 nm and ≈ 4 nm, thick, respectively. The PVA layer was rubbed by hand bidirectionally 30 times on velvet. The slow dynamic responses of the PVA and of

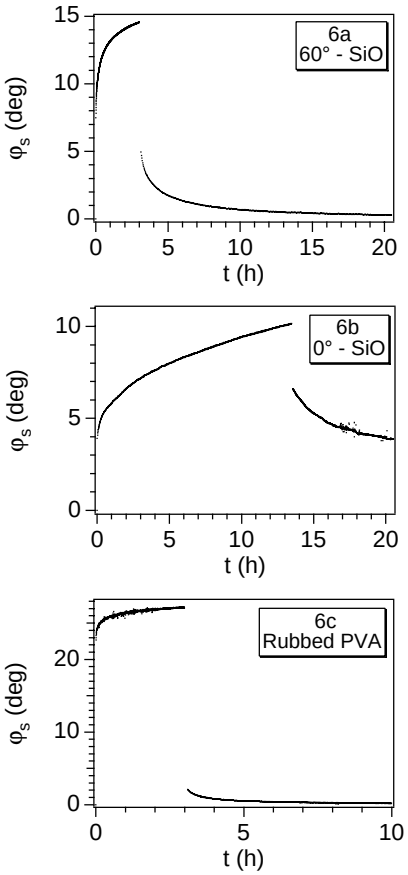

Fig. 6. Time behavior of the surface azimuthal angle φ_s at the switching on and off of a 0.75 T magnetic field for three different substrates at the same temperature $T = 30°C$. $t = 0$ is the time of switching on of the magnetic field. (a) refers to a 60°-evaporated SiO substrate. H is switched off at $t = 3$ h. (b) refers to a 0°-evaporated SiO substrate. H is switched off at $t = 13$ h. (c) refers to a PVA rubbed substrate. H is switched off at $t = 3$ h.

the 0°-SiO substrates are still well fitted by a stretched exponential law for any temperature and magnetic field amplitude. The anchoring amplitude in Figure 6 is minimum for the 0°-SiO substrate and maximum for the PVA substrate. Then, the 0°-SiO substrate has the strongest anchoring energy. However, the anchoring energy comparison between the 0°-SiO and the other substrates (60°-SiO and rubbed PVA) must be taken with caution. Indeed, the azimuthal anchoring energy of 60°-SiO and of PVA rubbed substrates depends on the SiO layer thickness [15] and the rubbing parameters [32]. In reference [15] it was found that SiO-layers treated by oblique evaporation at 60° with a thickness higher than 10 nm have an anchoring energy comparable with that of the 0°-SiO layer in Figure 6b. This is a surprising result because, the director anchoring of the 0°-SiO layer is not an intrinsic property of the substrate but is induced by the magnetic field during the preparation procedure. The switching off curves for the intrinsically anisotropic substrates (60°-SiO and PVA) and for the 0°-SiO substrates show a similar slow dynamics but also an important qualitative difference. For the first kind of substrates, the surface director angle tends to approach the initial state ($\varphi_s = 0$), while for the 0°-SiO substrate, the surface angle approaches a finite equilibrium angle $\varphi_s \approx 3°$. This feature can be easily understood as the easy axis for the intrinsically anisotropic substrates is a well defined parameter which reflects the topological and physical anisotropy of the substrate, while, in the 0°-SiO case, the easy axis is not related to any intrinsic anisotropy of the substrate.

5 Discussion

The azimuthal anchoring which is induced by the magnetic field on a 0°-SiO substrate can be explained in terms of the presence of an anisotropic layer of adsorbed nematic molecules on the surface. A direct influence of the magnetic field on the topology of the substrate seems to be unlikely for this kind of hard substrates. Starting from an initial isotropically adsorbed distribution of molecules, two mechanisms could explain the occurrence of an anisotropic adsorbed layer: 1) the magnetic field alignes the nematic molecules close to the boundaries and, consequently, adsorption of nematic molecules with the long axes parallel to the magnetic field is favored if the surface is not saturated; 2) the bulk nematic molecules near to the surface exert an orienting torque on the surface adsorbed molecules which favors their orientational diffusion toward an axis parallel to the magnetic field. Both these mechanisms lead to the formation of an anisotropic adsorbed layer which exerts an anchoring torque on the nearest bulk nematic molecules. It is sufficient a very small anisotropy of the surface adsorbed layer to break the isotropy of the surface and generate an azimuthal anchoring for the director. A similar mechanism was considered to be responsible for the azimuthal anchoring induced by a nematic flow [8] on the same kind of substrate.

Concerning the 60°-SiO substrate, electron microscopy shows that the surface is characterized by parallel SiO-grooves which lead to an in-plane anisotropy. The homogeneous alignment of the director along the surface grooves is usually ascribed to the elastic Berreman mechanism. The basic assumption of the Berreman model is that the physico-chemical interactions between the nematic LC and a SiO substrate favor a planar director orientation with local arbitrary azimuthal orientations. This means that, from a microscopic point of view, the NLC molecules are free to assume any orientation on the surface plane. A director orientation which is not parallel to the surface grooves induces an interfacial distortion of the director field with a consequent excess of interfacial free energy [5]. It results a macroscopic azimuthal anchoring along the surface grooves due to the elastic properties of the liquid crystal.

The assumption that nematic molecules can rotate freely at the surface is a basic requisite for the Berreman model, but it seems to be in disagreement with the experimental results. Indeed, according to Yokoyama *et al.* [8], the 0° and the 60°-SiO substrates should have exentially the same microscopic physico-chemical nature.

This conjecture is supported by the experimental observation that these substrates show the same wall-induced pretransitional birefringence and the same contact angles for nematic LCs [8]. Therefore, an anisotropic adsorbed layer is expected to be also present on the 60°-SiO substrates and to affect the anchoring. Our experimental observations are in a good agreement with the Yokoyama *et al.* conclusions. As a matter of fact, 60°-SiO substrates and 0°-SiO substrates with the same thickness have virtually the same anchoring energies. This suggests strongly that similar mechanisms are responsible for the azimuthal anchoring of these substrates. In the case of the 60°-SiO substrates, the Berreman mechanism could be responsible of the initial homogeneous director alignment which is needed for the occurrence of an anisotropic adsorbed layer. In this context, it would play the same role of the orienting magnetic field which is used to induce an azimuthal easy axis on the isotropic 0°-SiO substrates. Note that in the literature there are already reported many experimental observations which demonstrate the relevance of memory phenomena for the surface director alignment [7,8,12–15,33–39].

The observation of a slow dynamic regime for the three qualitatively different substrates investigated in this work is a further demonstration of the relevance of adsorption phenomena for the azimuthal anchoring of nematic liquid crystals. Our experimental results can be explained by assuming that an anisotropic layer of nematic liquid crystal molecules is present on the surface. Let be $n(\gamma)$ the number of nematic molecules adsorbed on the substrate which are oriented with the azimuthal angle γ. The anchoring energy due to the adsorbed molecules is

$$W(\varphi_{\rm s}) = \int_0^{2\pi} W(\varphi_{\rm s},\gamma){\rm d}\gamma. \tag{13}$$

Here, for simplicity, we assume $W(\varphi_{\rm s},\gamma)$ has the Rapini-like form [40]

$$W(\varphi_{\rm s},\gamma) = \frac{a}{2} n(\gamma)\sin^2(\varphi_{\rm s}-\gamma), \tag{14}$$

where a is a constant. Substituting equations (14) in equation (13), after straightforward calculations we get

$$W(\varphi_{\rm s}) = \frac{K_{22}}{L}\sin^2(\varphi_{\rm s}-\varphi_{\rm e}). \tag{15}$$

In equation (15) we have omitted an unexential additive constant. L and $\varphi_{\rm e}$ are the extrapolation length and the easy azimuthal angle and are explicitly given by:

$$L = \frac{K_{22}}{\sqrt{(A-B)^2+C^2}} \tag{16}$$

and

$$\varphi_{\rm e} = \frac{1}{2}\arctan\left(\frac{C}{A-B}\right), \tag{17}$$

where A, B and C are defined by

$$A = \int_0^{2\pi} \frac{a}{2} n(\gamma)\cos^2\gamma{\rm d}\gamma, \tag{18}$$

$$B = \int_0^{2\pi} \frac{a}{2} n(\gamma)\sin^2\gamma{\rm d}\gamma, \tag{19}$$

$$C = \int_0^{2\pi} a n(\gamma)\cos\gamma\sin\gamma{\rm d}\gamma. \tag{20}$$

The anchoring parameters in equations (16) and (17) have been obtained assuming that the adsorbed layer is the only mechanism of azimuthal anchoring. In the case of the intrinsically anisotropic substrates (60°-SiO substrates and PVA substrates), the anchoring energy is expected to be the sum of two contributions: the anchoring energy in equation (15) due to adsorbed molecules and an other term due to the intrinsic azimuthal anchoring (elastic Berreman mechanism, direct interactions with the polymeric chains). If we neglect the surface viscosity (see Sect. 3), the director angle has to satisfy the boundary condition

$$K_{22}\left.\frac{\partial\varphi}{\partial z}\right|_{z=0} = \frac{K_{22}}{2L}\sin 2(\varphi_{\rm s}-\varphi_{\rm e}), \tag{21}$$

which establishes the equilibrium of the surface elastic and anchoring torques. $\varphi = \varphi(z,t)$ in equation (21) is the solution of the bulk Leslie-Enricksen dynamic equation for the director (Eq. (4)). Parameters L and $\varphi_{\rm e}$ in equations (16, 17) depend on the distribution $n(\gamma)$ of the adsorbed molecules. In the absence of the desorienting magnetic field, the adsorbed molecules are preferentially oriented at the angle $\gamma = 0$. If $n(\gamma)$ satisfies the symmetry condition $n(\gamma) = n(-\gamma)$, the easy angle is $\varphi_{\rm e} = 0$. At the switching on of a desorienting magnetic field, the bulk molecules near to the surface turn toward the field direction and reach a new average surface angle $\varphi_{\rm s} \neq 0$. In this condition, the desorption of nematic molecules oriented along the initial easy axis ($\varphi_{\rm e} = 0$) and the successive adsorption of molecules oriented at the angle $\varphi_{\rm s}$ is favored. Another possibility consists on the anisotropic orientational diffusion of the adsorbed molecules driven by the surface elastic torque toward the field direction. Both these mechanisms lead to a time-variation of the distribution $n(\gamma)$ of the adsorbed molecules with a consequent variation of parameters L and $\varphi_{\rm e}$ in equations (16, 17). The time scales involved in these processes are expected to be much greater than the bulk relaxation time $\tau_{\rm b}$. This means that, during the short bulk relaxation, both L and $\varphi_{\rm e}$ remain virtually constant. Then, the fast dynamics of the surface and bulk director field is well described by the classical theory where L and $\varphi_{\rm e}$ are parameters independent of time, in agreement with the experimental results in Section 3. At times $t \gg \tau_{\rm b}$, the bulk director field has reached a virtually stationary configuration, and the slow time-variation of parameters L and $\varphi_{\rm e}$ in equation (21) cannot be disregarded. Since the characteristic time of this variation is much greater than τ_b, the bulk director field follows adiabatically the surface reorientation. This means that the bulk director field at time t is well approximated by the equilibrium configuration which minimizes the free energy for the corresponding surface angle $\varphi_{\rm s}(t)$. Then, the elastic torque appearing in the l.h.s. in equation (21)

can be replaced with the equilibrium surface elastic torque $\Gamma_{\rm e} = K_{22}\cos\varphi_{\rm s}/\xi_{\rm H}$, and equation (21) becomes

$$\cos\varphi_{\rm s} = \frac{\xi_{\rm H}}{2L}\sin 2(\varphi_{\rm s} - \varphi_{\rm e}). \tag{22}$$

For small values of $\varphi_{\rm s}$ and $\varphi_{\rm e}$, we get:

$$\varphi_{\rm s} = \varphi_{\rm e} + \frac{L}{\xi_{\rm H}}, \tag{23}$$

where L and $\varphi_{\rm e}$ are, now, slow functions of time. Equation (23) shows that the time-variation of $\varphi_{\rm s}$ is due to two different contributions: a gliding of the easy axis $\varphi_{\rm e}$ and a time-variation of the extrapolation length L. Both these variations are due to the very slow changes of density $n(\gamma)$ of the adsorbed molecules. The construction of a specific model for the time-evolution of density $n(\gamma)$ of the adsorbed molecules which satisfies the experimental observations is a still open problem. More information on the mechanisms of anisotropic adsorption of nematic molecules are needed.

6 Conclusions

In conclusion, the surface reorientation dynamics of the surface director angle on qualitatively different substrates has been investigated. The substrates used give all an homogeneous planar anchoring. They are obtained by rubbing PVA, by 60° SiO evaporation and by 0° SiO evaporation followed by a curing preparation in the presence of an orienting magnetic field. For all the substrates, the experimental results demonstrate the existence of a similar very slow dynamics with a strongly non-exponential character which cannot be explained in terms of the conventional anchoring mechanisms. Moreover, the 0°-SiO substrate shows an azimuthal anchoring energy comparable with that of the traditional intrinsically anisotropic substrates (60°-SiO, rubbed PVA). The presence of a similar slow dynamics and of comparable anchoring energies suggests strongly that an anisotropic surface layer of adsorbed nematic molecules can give an important and, perhaps, decisive contribution to the azimuthal director anchoring.

References

1. P.G. de Gennes, *The Physics of Liquid Crystals* (Clarendon, Oxford, 1974).
2. H. Yokoyama, Mol. Cryst. Liq. Cryst. **165**, 265 (1988).
3. S. Faetti, in *The Physiscs of Liquid Crystalline Materials*, edited by I.C. Khoo, F. Simoni (Gordon and Breach Science Publishers, Philadelphia, 1991).
4. S. Ishihara, H. Wakemoto, K. Nakazima, Y. Matsuo, Liq. Cryst. **4**, 669 (1989).
5. D.W. Berreman, Phys. Rev. Lett. **28**, 1683 (1972).
6. S. Faetti, Phys. Rev. A **36**, 408 (1987).
7. J. Cheng, G. D. Boyd, Appl. Phys. Lett. **35**, 444 (1979).
8. H. Yokoyama, S. Kobayashi, H. Kamei, J. Appl. Phys. **56**, 2645 (1984).
9. B. Jerome, P. Pieranski, J. Phys. France **49**, 1601 (1988).
10. R. Barberi, I. Dozov, M. Giocondo, M. Iovane, Ph. Martinot-Lagarde, D. Stoenescu, S. Tonchev, L.V. Tsonev, Eur. Phys. J. B **6**, 83-91 (1998).
11. E.A. Olivera, A.M. Figueiredo Neto, G. Durand, Phys. Rev. A **44**, R825 (1991).
12. T. Nose, S. Masuda, S. Sato, Jpn. J. Appl. Phys. **30**, 3450 (1991).
13. Y. Sato, K. Sato, T. Ushida, Jpn. J. Appl. Phys. **31**, L579 (1992).
14. V.P. Vorflusev, H.S. Kitzerow, V.G. Chigrinov, Appl. Phys. Lett. **70**, 3359 (1997).
15. S. Faetti, M. Nobili, A. Schirone, Liq. Cryst. **10**, 95 (1991).
16. A.I. Derzanski, A.G. Petrov, Acta Phys. Pol. **A55**, 747 (1979).
17. G. Durand, G.Virga, Phys. Rev. E (in press).
18. P. Galatola, G. Barbero, A.K. Zvezdin, Phys. Rev. E **55**, 4314 (1997).
19. S. Faetti, M. Nobili, Phys. Lett. A **217**, 133(1996).
20. J. Cognard, Mol. Cryst. Liq. Cryst. Suppl. **1**, 1 (1982).
21. S. Faetti, M. Nobili, Liq. Cryst. **25**, 487 (1998).
22. W. Urbach, M. Boix, E. Guyon, Appl. Phys. Lett. **25** 479 (1974).
23. S. Faetti, V. Palleschi, A. Schirone, Il Nuovo Cimento D **10**, 1313 (1988).
24. S. Faetti, M. Nobili, I. Raggi, J. Phys. II France **4**, 287 (1994).
25. G. Barbero, E. Miraldi, C. Oldano, M.L. Rastrello, P. Taverna Valabrega, J. Phys. France **47**, 1411 (1986).
26. I. Lelidis, M. Nobili, G. Durand, Phys. Rev. E **48**, 3818 (1993).
27. J.H. Coles, M.S. Stefan, Mol. Cryst. Liq. Cryst. **36**, 51 (1976).
28. J.D. Bunning, T.E. Faber, P.L. Sherrel, J. Phys. France **42**, 1175 (1981).
29. H.J. Coles, C. Strazielle, Mol. Cryst. Liq. Cryst. **55**, 273 (1979).
30. B.R. Ratna, P. Shashidhar, Mol. Cryst. Liq. Cryst. **42**, 113 (1977).
31. P. Pieranski, F. Brochard, E. Guyon, J. Phys. France **34**, 35 (1973).
32. T. Oh-Ide, S. Kuniyasu, S. Kobayashi, Mol. Cryst. Liq. Cryst. **164**, 91 (1988).
33. N. Koshida, S. Kikui, Appl. Phys. Lett. **40**, 541 (1982).
34. H.A. van Sprang, Mol. Cryst. Liq. Cryst. **97**, 255 (1983).
35. N.A. Clark, Phys. Rev. Lett. **55**, 292 (1985).
36. Y. Ouchi, M.B. Feller, T. Moses, Y.R. Shen, Phys. Rev. Lett. **68**, 3040 (1992).
37. B.O. Myrvold, Liq. Cryst. **18**, 287 (1995).
38. Y. Ouchi, M.B. Feller, T. Moses, Y.R. Shen, Phys. Rev. Lett. **68**, 3040 (1992).
39. M. Nobili, R. Barberi, G. Durand, J. Phys. II France **5**, 531 (1995).
40. A. Rapini, M. Papoular, J. Phys. Colloq. France **30**, C4-54 (1969).